Acta Cryst. (1993). D**49**, 75–85

Entropy Phase Dynamics

BY A. D. MCLACHLAN

Medical Research Council Laboratory of Molecular Biology, Hills Road, Cambridge CB2 2QH, England

(*Received* 22 *June* 1992; *accepted* 27 *July* 1992)

Abstract

The entropy-dynamics method seeks maxima for the entropy of the electron density for N atoms in a crystal cell, when the Fourier amplitudes are fixed, but their phases are unknown. By analogy with molecular dynamics, the effective potential energy is the negative entropy $V = -NS$. The kinetic energy is proportional to the squared velocities of the electron densities at grid points in the map. It reduces to a sum of Fourier-mode rotor energies. Each rotor angle experiences a couple equal to the phase gradient of S, and local dynamical equilibrium yields a Boltzmann distribution of S. Discrete phase angles (*e.g.* signs) are treated as quantized rotor modes. The distributions depend on a *popularity* function of the entropy histogram. Trial calculations have been made of phase averages and correlations in a centrosymmetric projection of the membrane protein bacteriorhodopsin. The maximum-entropy solution and the correct solution do not always coincide.

1. Introduction

The well known maximum-entropy method for refining electron-density maps (Gull & Daniell, 1978; Collins, 1982; Wilkins, Varghese & Lehmann, 1983; Skilling & Bryan, 1984; Gull, Livesey & Sivia, 1987) assumes that the most probable set of phases consistent with given structure-factor amplitudes from a random collection of atoms is the set which yields the density map with the highest entropy. This criterion is closely related to the triplet, quartet and higher cluster probability distributions used in small-molecule direct methods (Karle & Hauptman, 1950; Klug, 1958; Giacovazzo, 1980; Bricogne, 1984). The calculation of a maximum-entropy map with fixed guide phases for a given limited set of reflections is easy (Collins, 1982; Levine, 1980; Gull & Daniell, 1978; Navaza, 1985; Prince, Sjölin & Alenljung, 1988; McLachlan, 1989; Bricogne & Gilmore, 1990) but difficult problems remain.

(i) The entropy function has many maxima, sometimes separated by deep minima (for example, between two enantiomorphs).

(ii) Procedures for optimizing the phases (for example, Newton–Raphson steps, conjugate gradients, least squares) usually terminate at the nearest maximum.

(iii) The many entropy maxima must, therefore, be explored from several starting points.

(iv) There have been no systematic studies to verify, even in the simplest cases, whether the maximum-entropy phase set is the same as, or close to, the correct solution.

Most successful phasing procedures now use multiple solutions: random starts (Sheldrick, 1990; Sjölin, Prince, Svensson & Gilliland, 1991), magic integers (White & Woolfson, 1975; Main, 1977; Giacovazzo, 1980) or tree searches (Gilmore, Bricogne & Bannister, 1990; Dong *et al.*, 1992). Simulated annealing (Kirkpatrick, Gelatt & Vecchi, 1983; Sheldrick, 1990; Subbiah, 1991) has been used to explore both reciprocal space and real space.

The problem of multiple solutions occurs in other fields, especially in calculations of the structure of protein molecules in solution. Here, the energy (or free energy) has enormous numbers of local minima (Levinthal, 1968; Levitt, 1982). Monte Carlo methods, simulated annealing and molecular dynamics (McCammon & Harvey, 1987; Allen & Tildesley, 1987) are now powerful tools for exploring protein conformations.

In this paper the object is to apply a similar dynamical approach to the exploration of entropy maxima in the space of phases. The essence of the method is to introduce a fictitious *entropic temperature* and a fictitious kinetic energy for the system of unknown phases. The kinetic energy acts as a heat reservoir which allows the phases to move freely between adjacent entropy maxima. The fictitious potential energy is the negative entropy.

Here we outline the basic principles of phase dynamics and describe simple test calculations on a small centrosymmetric object, the two-dimensional projection of the membrane protein bacteriorhodopsin (Bullough & Henderson, 1990; Henderson & Unwin, 1975). These tests suggest that dynamics is useful for exploring the neighbourhood of a starting phase set. Enumeration of all possible phases for the strongest reflections shows that, although the correct solution

0907-4449/93/010075-11$06.00

is not the same as the maximum-entropy solution, it does lie near the top of the distribution of entropies taken over all possible phase sets.

2. The rotor model

2.1 *Monte Carlo methods and molecular dynamics*

Entropy dynamics, like molecular dynamics, executes a Brownian motion over the accessible neighbourhood of the current phase variables, moving continually from one maximum to another.

The simplest molecular simulation is the Monte Carlo method, typified by the Metropolis algorithm (Metropolis, Rosenbluth, Rosenbluth, Teller & Teller, 1953; McCammon & Harvey, 1987; Allen & Tildesley, 1987). At any instant the system has an energy E and a temperature T. A possible move is then considered in which certain atoms would have given displacements and the energy would increase by a predicted amount ΔE. If ΔE is negative the move must always be accepted: if ΔE is positive the acceptance is random, with a probability $p = \exp(-\Delta E/kT)$, where k is Boltzmann's constant. During a long succession of trials the system passes through every state, staying in each one for a fraction of the moves given by the Boltzmann distribution law $f(E) = A\exp(-E/kT)$, where A is a normalizing factor. Simulated annealing procedures (Kirkpatrick, Gelatt & Vecchi, 1983) are used to control the temperature: successive graduated cycles of heating and cooling tend to lead eventually to the global energy minimum

In classical molecular dynamics N atoms, as particles with positions $\mathbf{r}_a$ and velocities $\mathbf{v}_a$, move under a known potential energy function $V(\mathbf{r}_1, \mathbf{r}_2, ...\mathbf{r}_N)$. Typical components of V are bond stretching, valence-angle bending, torsion angles, van der Waals and electrostatic energy terms. Each atom also has a kinetic energy $\frac{1}{2}m_a\mathbf{v}_a^2$, where m_a is its mass, and so the total energy is the sum of V and the kinetic energy W: $E = V(\mathbf{r}) + W$. The laws of statistical mechanics (Hill, 1956; Tolman, 1938) show that in assemblies of many atoms the energy of the microcanonical ensemble is conserved. The system relaxes to a state of thermal equilibrium at a temperature T, where each kinetic degree of freedom has a mean energy of $\frac{1}{2}kT$. The temperature can be controlled over a period of time by adjusting the kinetic energy to its expected value $W = \frac{3}{2}NkT$, and Boltzmann's law applies to any part of the system, with a distribution

$$f(\mathbf{r},\mathbf{v}) = A'\exp(-\textstyle\sum_a m_a\mathbf{v}_a^2/2kT)\exp[-V(\mathbf{r}_1,...\mathbf{r}_N)/kT]. \tag{2.1}$$

Although the total energy is conserved the kinetic and potential energies separately both fluctuate, and the potential energy alone has the Boltzmann distribution $f(\mathbf{r}) = A''\exp[-V(\mathbf{r})/kT]$. The system is able to jump over potential energy barriers with heights of order kT by borrowing kinetic energy from the molecular motions.

2.2. *Entropy dynamics*

In the maximum-entropy method (Jaynes, 1957*a*,*b*, 1983; Levine & Tribus, 1979) the asymptotic probability of a set of phases for N atoms distributed randomly within a unit cell is proportional to

$$f = \exp(NS) \tag{2.2}$$

when N is large. Here S is the entropy of the maximum-entropy density map generated by the prescribed Fourier amplitudes with given phases. We take the fictitious potential energy for the dynamical simulation as

$$V = -NS. \tag{2.3}$$

Then, in equilibrium at a certain entropic temperature, θ, Boltzmann's law will give a phase probability distribution proportional to

$$f = \exp(NS/\theta). \tag{2.4}$$

We specify the map as an atomic probability distribution p_j on a grid of L equally spaced lattice points in the cell, normalized to a sum of N rather than 1. Then

$$NS = -\sum_{j=1}^{L} p_j\log p_j, \quad \sum_j p_j = N. \tag{2.5}$$

Notice that here we ignore correction terms proportional to $N^{1/2}$ which come from the saddle-point approximation (Bricogne, 1984; Skilling, 1989). Also, if we had used the conventional probability $p_j' = p_j/N$ normalized to unity over the cell, the entropy $S' = -\sum_j p_j'\log p_j'$ would have been equivalent to S except for a constant ($S = S' - \log N$).

Next we assign to each grid point a fictitious velocity dp_j/dt and effective mass μ, giving an effective kinetic energy

$$W = \textstyle\sum_j \frac{1}{2}\mu(\mathrm{d}p_j/\mathrm{d}t)^2. \tag{2.6}$$

This reduces to a sum over independent normal modes by taking Fourier components of the velocities. Using a unitary transform we define coefficients

$$Q_\mathbf{h} = L^{-1/2}\textstyle\sum_j \exp(2\pi i\mathbf{h}.\mathbf{x}_j)p_j = R_\mathbf{h}\exp(i\varphi) = \alpha_\mathbf{h} + i\beta_\mathbf{h}. \tag{2.7}$$

Here the grid has (L_x, L_y, L_z) subdivisions along the three axes, and the point j with grid indices (j_x, j_y, j_z) has cell coordinates $\mathbf{x}_j = (x, y, z) = (j_x/L_x, j_y/L_y, j_z/L_z)$. The index j_x takes the values 0, 1, ...$(L_x - 1)$,

and so on. The kinetic energy reduces to

$$W = \sum_{\mathbf{h}} \tfrac{1}{2}\mu\left[\left(\frac{\mathrm{d}\alpha_{\mathbf{h}}}{\mathrm{d}t}\right)^2 + \left(\frac{\mathrm{d}\beta_{\mathbf{h}}}{\mathrm{d}t}\right)^2\right]$$

$$= \sum_{\mathbf{h}} \tfrac{1}{2}\mu\left(\frac{\mathrm{d}R_{\mathbf{h}}}{\mathrm{d}t}\right)^2 + \sum_{\mathbf{h}} \tfrac{1}{2}\mu R_{\mathbf{h}}^2\left(\frac{\mathrm{d}\varphi_{\mathbf{h}}}{\mathrm{d}t}\right)^2. \quad (2.8)$$

The radial term, proportional to $(\mathrm{d}R_{\mathbf{h}}/\mathrm{d}t)^2$, is only present when $|Q_{\mathbf{h}}|$ is changing, and vanishes when the amplitudes are fixed. The angular term depends on the rate of change of phase, and means that each mode, $\mathbf{h}$, behaves like a rotor with angular velocity $\omega_{\mathbf{h}} = \mathrm{d}\varphi_{\mathbf{h}}/\mathrm{d}t$ and an effective moment of inertia $I_{\mathbf{h}} = \mu|Q_{\mathbf{h}}|^2$. The equipartition theorem in statistical mechanics shows that in thermal equilibrium each rotor has an equal mean kinetic energy $\frac{1}{2}I_{\mathbf{h}}\omega_{\mathbf{h}}^2 = \frac{1}{2}\theta$. Thus the strong reflection phases tend to rotate slowly and the weak ones rapidly. Comparing the mode amplitude $Q_{\mathbf{h}}$ with the standard crystallographic amplitudes for equal point atoms

$$E_{\mathbf{h}} = N^{-1/2}\sum_{a=1}^{N} \exp(2\pi i\,\mathbf{h}.\mathbf{r}_a) \text{ or } U_{\mathbf{h}} = N^{-1/2}E_{\mathbf{h}}, \quad (2.9)$$

we see that when the grid distribution p_j reduces to N spikes there is a precise correspondence, with $Q_{\mathbf{h}} = (N/L)^{1/2}E_{\mathbf{h}} = (NL^{-1/2})U_{\mathbf{h}}$.

2.3. *Non-linear mixing of modes*

The lattice dynamics of an ideal real molecular crystal are described very well in terms of non-interacting normal modes, or phonons, which have a nearly quadratic potential energy. By contrast, the fictitious entropy potential function $-NS(\varphi_1,\varphi_2,\ldots\varphi_N)$ is a highly non-linear function of the phase invariants, involving the triplets, quartets and higher terms. So the modes are anharmonic: they become mixed together during the motion, because the angular couples acting on each rotor depend on the phases of other rotors that belong to its phasing neighbourhoods. Modes collide and scatter, exchanging energy with the reservoir of kinetic energy.

3. Mode dynamics

3.1. *Equations of motion*

We start with given phases $\varphi_{\mathbf{h}}$ and their angular velocities, $\omega_{\mathbf{h}}$. Each rotor has an angular momentum $J_{\mathbf{h}} = I_{\mathbf{h}}\omega_{\mathbf{h}}$, where the moment of inertia $I_{\mathbf{h}}$ is fixed, and it experiences a couple $C_{\mathbf{h}} = -\partial V/\partial\varphi_{\mathbf{h}}$. Thus the equations of motion are

$$(\mathrm{d}J_{\mathbf{h}}/\mathrm{d}t) = C_{\mathbf{h}} = N(\partial S/\partial\varphi_{\mathbf{h}})$$

$$= N[\alpha_{\mathbf{h}}(\partial S/\partial\beta_{\mathbf{h}}) - \beta_{\mathbf{h}}(\partial S/\partial\alpha_{\mathbf{h}})]. \quad (3.1)$$

The entropy gradients in (3.1) are the Lagrangian multipliers that belong to the standard maximum-entropy solution for the current phases (Gull & Daniell, 1978; Wilkins, Varghese & Lehmann, 1983) and are obtained immediately from the entropy-optimization process.

3.2. *Improper phases and modified entropy*

In practice, negative probability densities occur at various grid points when the postulated phase sets are physically impossible: that is when they cannot be represented by any configuration of point atoms. These non-physical sets should have zero probability, or infinitely negative entropy, but the classical entropy tends to zero as $p_j \to 0$ and does not exist for negative p_j. We use a modified entropy function, $S_m(p)$, with a 'badness penalty' for negative densities, which makes the potential energy $-NS$ very large at these grid points. We choose a small positive cut-off density p_m (*e.g.* $p_m = 0.01$), and then select either

$$S_m(p) = -p\log p,$$

if $p \geq p_m$, or

$$S_m(p) = -p_m\log p_m + (p_m - p)(1 + \log p_m) - (p_m - p)^2/p_m, \quad (3.2)$$

if $p < p_m$. The modified form is a quadratic function which matches the value and gradient of the classical entropy when $p = p_m$ and passes through $S_m(0) = 0$. Another useful entropy function is the Fermi–Dirac entropy, in which the particle density at each grid point cannot exceed unity: $S_{\mathrm{FD}}(p) = -p\log p - (1-p)\log(1-p)$. This has a similar modified form $S_{m\mathrm{FD}}(p) = [S_m(p) + S_m(1-p)]$.

3.3. *Approximating the maximum-entropy solution*

In practice it is expensive to compute a precise updated maximum-entropy map after each small phase increment, and we have used a gross approximation, which can be removed later: this is to hold all the inactive Fourier components fixed at zero amplitude. The result is that the estimated entropy is always below its correct optimal value.

3.4. *Discontinuous phases and stepped rotors*

Rotor dynamics is best suited to continuous phases, which include the majority of reflections in most space groups. This is because the stored kinetic energy of the rotor tends to drive the phase continuously through local energy maxima and explore the whole range of angles. The different angular velocities of the modes produce asynchronous sampling of the phase combinations.

In many space groups there are special reflections where the phases are restricted to certain fractions of

2π, or even to a sign (0 or π). Stepped phases are modelled by using a continuous rotor clock angle $\chi_{\mathbf{h}}$, with angular velocity $\omega_{\mathbf{h}}$, which carries the kinetic energy and trips the phase $\varphi_{\mathbf{h}}$ when it passes certain critical markers. The entropy is a step function which jumps at each marker. The dynamics behaves like a classical particle colliding with a potential energy barrier. If the rotor has sufficient kinetic energy to jump over an upward potential energy step, it continues with reduced angular velocity. Otherwise the rotor is reflected backwards.

Fig. 1 illustrates the use of a clock angle for a centrosymmetric reflection with allowed phases of 0 and π. When χ lies between $+\pi/2$ and $-\pi/2$ the phase is $\varphi = 0$, but it changes to $\varphi = \pi$ on passing these markers. The dynamics of centrosymmetric phases is almost equivalent to a two-state Monte Carlo flip. The main differences are that the clock

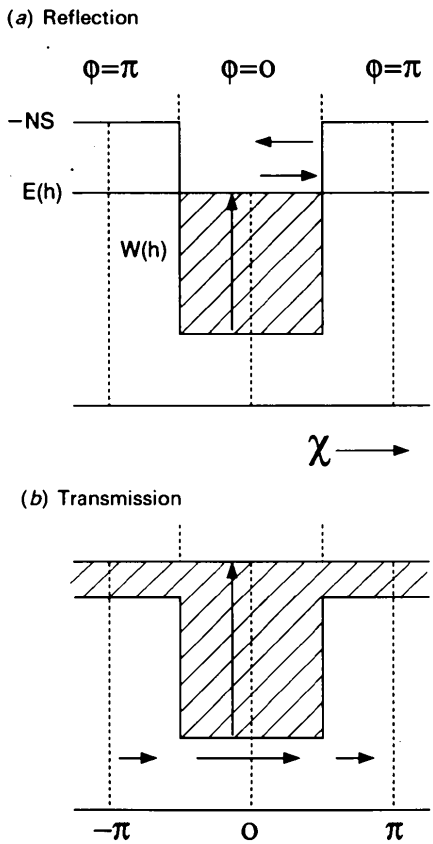

Fig. 1. Dynamics of a stepped rotor with allowed phases $\varphi_{\mathbf{h}} = 0$ or π. The phase jumps when the clock angle $\chi_{\mathbf{h}}$ passes the markers at $\pi/2$ and $-\pi/2$. The total energy available to the rotor, $E(\mathbf{h})$, is the sum of $-NS$ and the kinetic energy $W(\mathbf{h}) = \frac{1}{2}(I_{\mathbf{h}}\omega_{\mathbf{h}}^2)$. In (*a*) the kinetic energy is too small to overcome the entropy step and the motion is reflected at each marker. The phase remains trapped at $\varphi_{\mathbf{h}} = 0$. In (*b*) the rotor slows down at the step but continues with a reduced angular velocity. The phase alternates between 0 and π.

angles determine the order of the flips in time, and the potential energy gives a causally determined outcome to each event.

The stepped-rotor model applies to any number of restricted phase angles, and is a useful approximation for treating the motion of continuous phases. It ensures that the fictitious energy is conserved at all times.

3.5. *Sign flip entropies*

With a centrosymmetric object, the entire motion reduces to a succession of sign flips, one mode at a time. It is also possible to control the selection of active modes. At any time a mode may be either clamped with a fixed sign, rotating, or switched off, with an amplitude set to zero. Thus, considering a single mode $\mathbf{h}$ with all the other modes $\mathbf{k}$ set to signs $g_{\mathbf{k}}$, the variable sign $g_{\mathbf{h}}$ may take the three values 0, ± 1, with corresponding entropies $S_0(\mathbf{h})$, $S_+(\mathbf{h})$, $S_-(\mathbf{h})$ for the whole system. In an active mode the current actual sign may flip to the opposite value, and the subsequent motion depends on an important quantity, the *reversal entropy* defined as

$$S_{\text{rev}}(\mathbf{h}) = S_{\text{actual}}(\mathbf{h}) - S_{\text{opposite}}(\mathbf{h}) = \pm[S_+(\mathbf{h}) - S_-(\mathbf{h})]. \tag{3.3}$$

Another important event is the switching on of an inactive mode $\mathbf{h}$ from an initial amplitude of zero to its full current amplitude and positive or negative sign. The resulting 'switching-on entropies' are $S_{0+}(\mathbf{h})$ and $S_{0-}(\mathbf{h})$, where $S_{0+}(\mathbf{h}) = S_+(\mathbf{h}) - S_0(\mathbf{h})$ and $S_{0-}(\mathbf{h}) = S_-(\mathbf{h}) - S_0(\mathbf{h})$. Introducing a further constraint normally reduces the total entropy, hence $S_{0+}(\mathbf{h})$ and $S_{0-}(\mathbf{h})$ are usually both negative.

At a temperature θ the mean kinetic energy of each rotor is $\frac{1}{2}\theta$, and so modes with $|S_{\text{rev}}(\mathbf{h})| \gg \theta$ will tend to move into their maximum-entropy settings, with stable fixed phases, while those modes with $|S_{\text{rev}}(\mathbf{h})| \ll \theta$ will continue to flip rapidly. At an entropy maximum all modes will have positive values of $S_{\text{rev}}(\mathbf{h})$.

The actual calculation of the reversal entropy is simple, since it only involves changing one mode (a single Fourier component of density with its symmetry-related companions). The densities p_j are updated in one operation, and the entropies recomputed. After many updates the small rounding off errors in the density accumulate, and so a full fast Fourier transform of the amplitudes is carried out at intervals to correct for any drift.

3.6. *Undefined signs and likelihood*

In simple entropy dynamics every mode of interest has a well defined sign $g_{\mathbf{h}}$ and the effective potential energy is $V = -NS$. A more general Bayesian

approach is to take $V = -N\Lambda$, where $N\Lambda$ is the logarithm of the likelihood. The active modes are now split into two sets: a trial set $\mathbf{h}_1,...\mathbf{h}_H$, with H defined signs $(g_1...g_H)$, and a fluctuating set $\mathbf{k}_1...\mathbf{k}_K$ with K undefined signs $(l_1...l_K)$. We wish to calculate the likelihood of the trial set signs, averaged over all possible signs in the fluctuating set and weighted with their correct probabilities. The joint probability of a complete set of $(H + K)$ signs g and l is proportional to

$$f(g{:}l) = \exp[NS_{HK}(g{:}l)] \tag{3.4}$$

and is equal to the product of the prior probability of the signs l, times the conditional probability of g given l. So Bayes' theorem (Press, 1989) gives a log likelihood

$$\exp[N\Lambda_H(g)] = (1/Y)\exp[N\Lambda_{HK}(g)]$$
$$Y = \sum_g \exp[N\Lambda_{HK}(g)], \tag{3.5}$$

where

$$\exp[N\Lambda_{HK}(g)] = \sum_{l=\pm 1} \exp[NS_{HK}(g{:}l)] \tag{3.6}$$

summed over all sign combinations of $l_1...l_K$.

A full calculation of $\Lambda_H(g)$ for fixed values of the trial signs g often involves an impracticably large sum over 2^K sign combinations of l in the fluctuating set, but a simple approximation is possible. We start from a reference state in which all the fluctuating amplitudes are zero and where the reference entropy is $S_H(g) = S_{HK}(g_1...g_H{:}0...0)$. The full entropy $S_{HK}(g{:}l)$, with the fluctuating signs switched on, can be expressed exactly as a polynomial in the signs $(l_1...l_K)$. Since $l_j^2 = 1$ the polynomial only contains l_j with powers of 0, 1 and 2, and consists of 3^K terms, in which $S_H(g)$ is the constant part (powers all zero):

$$S_{HK}(g{:}l) = S_H(g) + \sum_{n=0,\,1,\,2}{}' X(g)_{n_1 n_2 ... n_K} l_1^{n_1} l_2^{n_2} ... l_K^{n_K}. \tag{3.7}$$

The $X(g)$ coefficents describe the entropy changes for switching on singlets, doublets, triplets *etc.* of fluctuating signs out of the reference state $(g{:}0)$. For example, the singlet terms in sign l_1 describe the switching-on entropies of mode $\mathbf{k}_1$ by itself with the trial set already fixed and all the other fluctuating modes turned off.

$$S_{0+}(\mathbf{k}_1) = X(g)_{10...0} + X(g)_{20...0}$$
$$S_{0-}(\mathbf{k}_1) = -X(g)_{10...0} + X(g)_{20...0}. \tag{3.8}$$

The approximation consists in neglecting all doublet, triplet and higher terms, even the quadratic cross terms such as $X(g)_{11...0} l_1 l_2$. Then the log likelihood becomes

$$\Lambda_{HK}(g) = S_H(g) + \sum_{j=1}^{K} \lambda_j(g) \tag{3.9}$$

with

$$\exp[N\lambda_j(g)] = \exp[NS_{0+}(\mathbf{k}_j)] + \exp[NS_{0-}(\mathbf{k}_j)]. \tag{3.10}$$

This approximation is analogous to the diagonal quadratic approximation (Bricogne, 1988; Gilmore Henderson & Bricogne, 1991), in which cross terms between different modes are neglected. The likelihood corrections λ_j can each be calculated from the reference state by making two sign flips of the mode $\mathbf{k}_j$, or else from a quadratic approximation to the entropy.

3.7. *Making a dynamics run*

An entropy-dynamics run involves several stages. The start up, the main run and the conclusion. In the start-up stage the active rotor modes are selected, usually with a choice between clamped phases, rotating phases and inactive terms (zero amplitude). A starting temperature is chosen (usually by examining the reversal entropies of the rotating modes), then motion is initiated.

The main run consists of 'bursts' of a preset number of phase flip events at the current temperature, in which the rotor may be either transmitted or reflected at the marker point. The total fictitious energy is conserved throughout the burst. The states of highest entropy may be extracted and saved for further use, ignoring all solutions that are too similar to ones already found.

After a burst the temperature may be adjusted, the angular velocities reset, and the active modes reselected. For example, the best-determined phases might be clamped progressively, and the temperature lowered till a local absolute maximum of the entropy is reached. Here every mode is stable and no further motion is possible.

3.8. *Temperature control*

The starting temperature θ is often set high (*e.g.* $\theta = 100\langle|S_{\rm rev}|\rangle$) to randomize the signs, but later an automatic control is used. When the temperature is too high, almost all modes can flip freely and the time-averaged entropy does not increase: when it is too low, almost all modes are locked and movement ceases.

In the first level of temperature control we set upper and lower targets $\gamma_{\max}$ and $\gamma_{\min}$ for the fraction of rotors that flip in M events. If ρ flips are observed, and $\rho > M\gamma_{\max}$, the temperature is lowered by a certain ratio $\theta \rightarrow \theta/\varepsilon_\theta$, but if $\rho < M\gamma_{\min}$ the temperature is raised: $\theta \rightarrow \varepsilon_\theta\theta$. Typically, $\varepsilon_\theta = 1.5$ and $M = 500$ with $\gamma_{\max} = 0.5$ and $\gamma_{\min} = 0.25$.

The secondary control mechanism is to readjust the target ratios $\gamma_{\max}$ and $\gamma_{\min}$ when a temperature

Table 1. *Numbers of strong reflection amplitudes in projected bacteriorhodopsin at* 3.9 Å *resolution*

$|F|$ scaled to standard deviation of 1.0 (Bullough & Henderson, 1990).

Number of reflections	Lower limit of $\|F\|$
1	5.0
7	4.0
21	2.5
57	1.5
91	1.0
217	0.01

Table 2. *The* 21 *strongest reflections in bacteriorhodopsin, with reversal entropies and parities of* (h,k)

S_{rev} (arbitrary units) was calculated with other modes off.

Mode	$\|F\|$	S_{rev}	(h,k)	Even/odd
1	4.998	1.801	0,8	*EE*
2	4.954	0.536	0,4	*EE*
3	4.777	1.579	6,5	*EO*
4	4.716	1.998	2,6	*EE*
5	4.469	1.661	6,3	*EO*
6	4.372	−0.259	4,4	*EE*
7	4.231	8.615	1,2	*OE*
8	3.957	−0.268	4,6	*EE*
9	3.943	1.183	4,8	*EE*
10	3.523	−0.038	2,5	*EO*
11	3.449	4.363	1,9	*OO*
12	3.435	1.116	3,4	*OE*
13	3.333	−0.704	4,2	*EE*
14	3.276	−0.848	12,0	*EE*
15	3.211	0.231	5,3	*OO*
16	3.051	0.842	6,0	*EE*
17	2.896	0.609	5,2	*OE*
18	2.869	0.043	5,1	*OO*
19	2.857	−0.508	2,2	*EE*
20	2.698	0.991	5,4	*OE*
21	2.571	2.129	8,0	*EE*

plateau is detected (a plateau is recognized when the moving average of the temperature becomes close to the current value). For example a reduction of both ratios by a common factor, ε_γ, at each plateau leads to a gradual forced cooling with an ultimate state of maximum entropy for all the rotating modes. The primary and secondary controls are reliable and effective, but not always economical, since they work by monitoring the sign flip rate in a succession of bursts.

4. Trial calculations

4.1. *Orthorhombic bacteriorhodopsin*

A suitable test object is the purple membrane proton-pump protein bacteriorhodopsin from *Halobacterium halobium* (Henderson & Unwin 1975; Henderson, 1977). The orthorhombic form of the membrane (space group $P2_12_12$: cell dimensions a = 58.70, b = 75.49, c = 100.50 Å), in projection at 3.9 Å resolution, has been solved by electron-microscope imaging (Bullough & Henderson, 1990). The image, with two-dimensional symmetry *pgg*, yields 220 experimentally phased reflections with an average phase error of 34.7°. The cell contains four copies of the seven-helix protein subunit, with the helical rods viewed end on.

The initial aim was to test the dynamics algorithm with a small number of strong reflections. We sorted the amplitudes of the strong reflections in order and scaled each $|F|$ to a minimum of zero and a standard deviation of unity (Table 1). The 21 strongest reflections, with amplitudes of 2.5 or more, give a useful trial set. This initial set is rather unbalanced for refinement purposes because it contains 11 modes of the *EE* parity group (Table 2).

We began by setting the 21 strong signs to their correct experimental values, with all other modes off (amplitude zero). Table 2 shows the reversal entropies $S_{rev}(h,k)$ of these strong modes, and the even/odd parities of h and k, which determine whether a sign changes under a half-cell shift of origin. Most of the S_{rev} values are positive, as expected for a maximum-entropy state, but six out of the 21 are negative. Evidently, the signs of the correct map are not the same as the maximum-entropy signs, given only these 21 amplitudes. However, if we set all the 217 modes with their correct signs and recalculate S_{rev} for the top 21 modes, the values now all become positive, and the entropy, based on more complete information, does have a true local maximum.

Fig. 2 shows the time course of a typical dynamics run. Here the 21 strong modes are rotating while the other background modes are clamped with their correct amplitudes and signs. In this run the temperature started at a high value and then evolved under automatic control through three successive

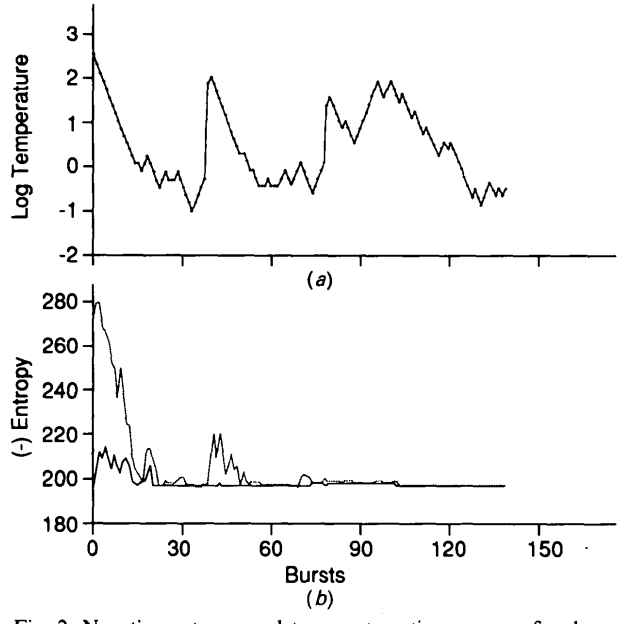

Fig. 2. Negative entropy and temperature time courses for dynamics with 21 rotating strong modes and the rest clamped. (*a*) Logarithmic plot of temperature θ in each burst of 100 events. (*b*) Entropy maxima and minima in each burst.

Table 3. *Census of entropies for the sign combinations of* 21 *strong reflections* (2 097 152 *sets*) *compared with the correct solution*

The correct solution is ranked against the sorted list of entropies. σ is the entropy scaled to a mean of 0.0 and standard deviation of 1.0 over each full set of sign combinations.

	Other modes	
	Clamped correct	Amplitude off
S(max)	−197.233	−145.893
S(min)	−343.037	−191.684
S(correct)	−197.233	−149.688
Position of correct solution	1	47884
σ(max)	2.717	2.265
σ(min)	−8.477	−9.918
σ(correct)	2.717	1.255

plateaux with decreasing flip rates, as explained above. The entropy graph is inverted, since $-NS$ corresponds to the fictitious potential energy of the system, which tends to a minimum. Notice how the entropy fluctuations decay rapidly as the modes settle into their equilibrium positions.

4.2. *Enumeration of sign combinations*

The next experiment was designed to test the relationship between the correct signs and the signs that yield entropy maxima. We enumerated all possible 2097152 sign combinations of the 21 strong modes by using the Gray code (Hamming, 1986). This sequence passes once through each state by flipping just one sign at a time, and is illustrated below for three signs:

Step	Binary digits d_k				Signs g_k		
	3	2	1	0	2	1	0
0	0	0	0	0	1	1	1
1	0	0	0	1	1	1	−1
2	0	0	1	0	1	−1	−1
3	0	0	1	1	1	−1	1
	...	...	...	...	...	...	...

Each binary number generates a sign set g_k from its ordered digits d_k by the rule: if $d_{k+1} = d_k$ then $g_k = 1$, otherwise $g_k = -1$. Addition of 1 to the current binary number leads to the next sign change at the left edge of the succession of 'carried' digits.

The enumeration was performed twice: once with all the other modes clamped at their correct signs, and once with all other modes switched off (Table 3). In the clamped test the correct solution corresponds exactly to the global entropy maximum (of the restricted rotating set). In the unclamped test the correct solution lies high in the distribution of observed entropies, but it is by no means the highest.

Another point of interest is the shape of the statistical distribution of the entropies over the large number of sign sets. This is most easily described by scaling the entropies in reduced units derived from the actual distribution with its mean of S_{av} and standard deviation S_{dev}. We define the reduced entropy $\sigma(g) = [S(g) - S_{av}]/S_{dev}$, and plot the histograms of σ in Fig. 3. These are strongly skewed curves with a rather steep and short tail on the high-entropy side and a long diffuse tail on the low-entropy side. The low side corresponds to the worst possible phase sets, where negative probability densities exist on many grid points.

4.3. *Entropic thermal equilibria*

When entropy dynamics is run for a long time at constant temperature, the entropy and the associated phases (or signs) reach a local fluctuating equilibrium. There is an entropic statistical mechanics which describes the distribution of entropy and phase in the fictitious model. Quantities of interest are the mean entropy, the mean values of the signs and the correlations between fluctuating signs. We work in terms of the reduced entropies $\sigma(g)$ and a reduced temperature $\tau = TS_{dev}/N$. The dynamical probability of a given sign combination g is then proportional to $\exp[\sigma(g)/\tau]$. We introduce two useful new quantities, the entropic partition function, $Z(\tau)$, and the statistical density of the histogram of σ, $\Omega(\sigma)$. This last is defined (see Fig. 3) so that the number of sign combinations which have entropy between σ and $\sigma + d\sigma$ is

$$dn = \Omega(\sigma)d\sigma. \tag{4.1}$$

The corresponding entropic partition function is

$$Z(\tau) = \sum_g \exp[\sigma(g)/\tau] = \int \Omega(\sigma)\exp(\sigma/\tau)d\sigma \tag{4.2}$$

integrated over the range σ_{min} to σ_{max}. The probability of any sign combination g in the motion becomes

$$f(g) = (1/Z)\exp[\sigma(g)/\tau] \tag{4.3}$$

and every dynamical average can then be calculated. The entropy density, Ω, is a very important quantity. First, as it derives from the scaled histogram, the allowed range of σ is effectively finite, of order ± 1, which implies that both positive and negative entropic temperatures can exist (Abragam, 1961). Second,

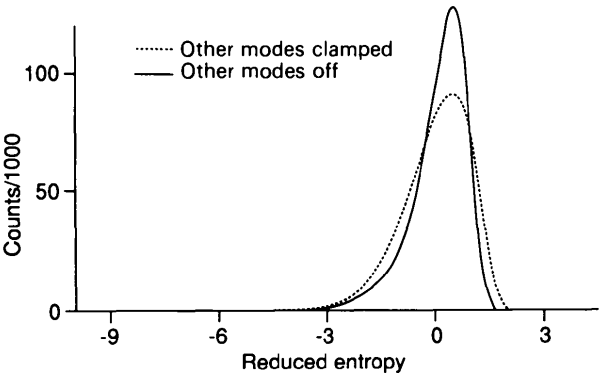

Fig. 3. Histograms of the scaled entropy $\sigma(g)$ for combinations of the 21 strong modes.

Table 4. *Thermal averages for* 21 *strong modes at a reduced temperature* $\tau = 0.1$

Modes are classified by even/odd parity of (h,k). Consensus signs $\langle g_i \rangle$ and sign correlation matrices $\langle g_i g_j \rangle$ are shown. Other modes are switched off. Values are multiplied by 10 and rounded to integers.

(*EE*) Modes

Mode number	1	2	4	6	8	9	13	14	16	19	21	
Averaged signs	−4	−5	−1	2	−1	−3	−1	−7	5	1	8	
Correlation matrix												
1	10	6	0	−4	0	1	0	3	−3	0	−3	−
2	6	10	1	−4	1	1	1	4	−4	−1	−4	−
4	0	1	10	−1	6	0	5	1	−1	−6	−1	−
6	−4	−4	−1	10	−2	−4	−1	−1	4	1	2	+
8	0	1	6	−2	10	0	6	1	−1	−5	0	−
9	1	1	0	−4	0	10	0	2	−2	−1	−2	−
13	0	1	5	−1	6	0	10	1	−1	−5	−1	−
14	3	4	1	−1	1	2	1	10	−4	−1	−6	−
16	−3	−4	−1	4	−1	−2	−1	−4	10	1	5	+
19	0	−1	−6	1	−5	−1	−5	−1	1	10	1	+
21	−3	−4	−1	2	0	−2	−1	−6	5	1	10	+

Correlation matrices for other parities

(*EO*) Modes

	3	5	10	
3	10	−3	4	+
5	−3	10	−2	−
10	4	−2	10	+

(*OE*) Modes

	7	12	20	17	
7	10	−1	−1	5	+
12	−1	10	6	−1	−
17	5	−1	0	10	+
20	−1	6	10	0	−

(*OO*) Modes

	11	15	18	
11	10	−1	−2	+
15	−1	10	2	−
18	−2	2	10	−

the logarithm of Ω is a fundamental thermodynamic variable of the system, which we call the *popularity* function for the given entropy:

$$\Gamma(\sigma) = \log \Omega(\sigma). \tag{4.4}$$

The number of times that a given value of the entropy is met during a dynamical run depends on the shape of the popularity histogram as well as the probability factor $\exp(\sigma/\tau)$. In large systems the mean equilibrium entropy $\langle \sigma(\tau) \rangle$ at temperature τ is the value of σ which maximizes

$$\psi(\sigma) = \sigma + \tau\Gamma(\sigma) \quad (\tau \text{ fixed}). \tag{4.5}$$

The quantity $\psi(\sigma)$ is analogous to the negative Helmholtz free energy ($-A = -U + TS$) in normal thermodynamics. Its maximum value is $\psi \simeq \log Z(\tau)$, and the condition for a maximum is that $d\Gamma/d\sigma = -1/\tau$. Thus a hypothetical normal distribution curve for Ω would give $\langle \sigma(\tau) \rangle = 1/\tau$.

This discussion makes it clear that a dynamics run will sample the sign sets in a way which depends on the popularity profile of the system. States near the entropy maximum are rare and have low popularities, so they may never be sampled if the temperature is too high.

The thermal averages $\langle g_i(\tau) \rangle$ from the vector of rotating signs $g = (g_1, g_2, \ldots g_H)$ give a consensus sign pattern. For example, when all the other modes are clamped at their correct phases, the 21 strong signs have mean values which depend on their reversal entropies. A complication is that normally most signs depend on the choice of cell origin, which is undefined when the remaining modes are unclamped, so that only the origin-independent set (parity *EE*) has a consensus sign, the rest averaging to zero. However, the cross-correlated averages of pairs of signs give a useful pair-correlation matrix, with elements $G_{ij}(\tau) = \langle g_i g_j \rangle_\tau$. The matrix divides into diagonal blocks for the different origin parity sets, and its eigenvectors describe the principal fluctuations of the signs at the given temperature. As an example, Table 4 illustrates the thermal averages for the 21 strong modes when $\tau = 0.1$ and all other modes are switched off. Each average value has been multiplied by 10 and rounded off. The right-hand column of each matrix shows the sign of the dominant eigenvector component in each group.

Thermal averages, based on many combinations, yield a much more consistent statistic for the signs than the unique signs of one selected high-entropy state.

4.4 *Progressive mode selection*

Once a small starting set of active modes has been tested, the dynamics run has gained some information about the most likely phases. To preserve and enlarge this information it is then useful to extend the active set. The most stable current modes (with large magnitudes of S_{rev}) may be clamped to preserve their good phases. We have tried several selection schemes. In each we assume that the modes have been sorted into groups of decreasing $|F|$ and that the reversal entropy $S_{\text{rev}}(\mathbf{h})$ is known.

(i) *Simple block extension.* The modes are divided into groups I, II, III, with group I as the starting set. In the second round all group I modes are clamped and group II modes rotated: in the third the group II modes are also clamped and group III modes rotated, and so on.

(ii) *Revision of unstable modes.* The least stable modes in a large starting set are rotated again in an iterative regime until the entropy ceases to increase.

(iii) *Alternate extension and revision.* Here the active set is alternately enlarged, by introducing a new group, and revised by clamping the current most stable modes, according to some rule. For example, the number of rotating modes may be successively reduced to the least stable 50, 25, 15%... of the active set.

Schemes (i) and (ii) have obvious weaknesses. In (i) there is no revision of the phases in earlier groups: in (ii) the starting set may be inconveniently large. Schemes similar to (iii) are more effective, but in practice the outcome of a dynamics run normally depends more on the fate of the early sign flips than on any ingenious later adjustments.

As an example, Fig. 4 shows the temperature and entropy time course of a typical long run in which the active set of modes has been enlarged according to scheme (i). The temperature passes through a series of plateaux, with a reheat whenever a new mode group is added. The entropy decreases sharply as each new group introduces further phase and amplitude constraints, but then settles into a new range of local maxima.

5. Discussion

The original objectives of this work were to find a way to explore maximum-entropy phase sets without becoming trapped in local maxima: to test whether the maximum-entropy solutions correspond to the known correct solutions in real situations; to try to solve the phases of a simple system *ab initio*, with the bacteriorhodopsin projection as a trial object.

5.1. *Practical trials*

The trials show that entropy dynamics is a feasible computational method, but is not yet powerful enough to solve a real structure. The equations of motion can be solved, the phases do not get trapped, and we can reach high-entropy solutions in a reasonable time. The practical enumeration of sign combinations shows that the dynamical averages at different entropic temperatures are an efficient way to summarize the most probable sets of phases; it is possible to rank the correct solution against the ensemble of different entropy values. A conventional entropy maximization on the same set of signs is almost equivalent to a near-zero temperature dynamics run, and trials with these (not described here) show that the run is a short random sequence of upward entropy steps, which becomes trapped at some fairly high local maximum.

The trials failed to find the correct solution in the restricted set of 21 strong reflections because the entropy target function has many higher values associated with incorrect sign combinations. A likelihood target function and a larger set of reflections may be needed to give more power.

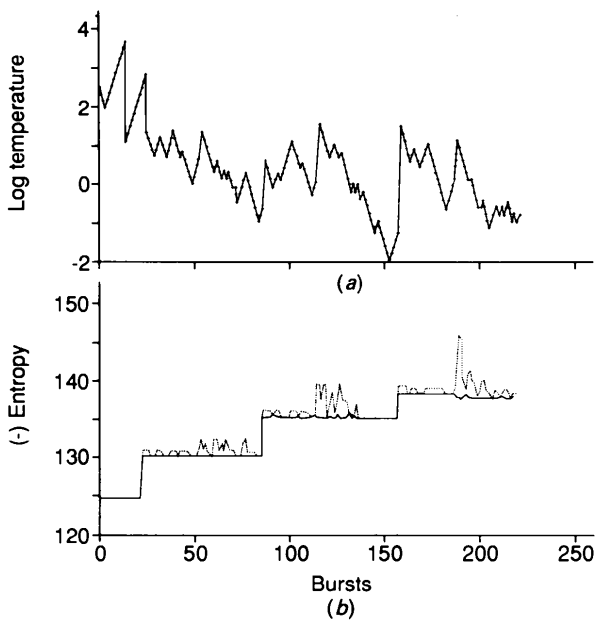

Fig. 4. A dynamics run with mode reselection. (*a*) Logarithmic plot of temperature θ in each burst of 100 events. (*b*) Entropy maxima and minima.

5.2. *Nature of the dynamical model*

In essence the approach is simple: to treat negative entropy as a fictitious potential energy, and rates of change of probability densities as velocities. The rotor angular momenta give the motion a directional persistence rather than a purely diffusive character. The notion of a clock angle that drives a stepped phase allows a discontinuous dynamics, essential for the special reflections. The rotor model defines the kinetic energy only, and it could be used with any other crystallographic driving potential such as the log likelihood, the residual in Sayre's equation, or the R factor.

5.3. *Executing the motion*

The rotor equations of motion are easy to solve, since they only need simple calculations of the entropy gradients for continuous rotations, or the flipping entropies at phase steps. The averages and fluctuations can be analysed by standard methods. In practical terms, entropy dynamics is as flexible and adaptable in use as other Monte Carlo procedures (*e.g.* Sheldrick, 1990). The simple automatic temperature control described in this paper effectively avoids local self-trapping.

5.4. *Thermal equilibria*

The well established principles of statistical mechanics provide a secure logical framework for interpreting the observed trajectories. The active degrees of freedom obey Boltzmann's distribution law, and the equipartition law for rotor kinetic energies. The notion of a transient entropic temperature equilibrium is helpful: the fluctuating phases and phase correlations depend strongly on the overall shape of the entropy histogram taken over the ensemble of phase sets. Here the popularity, $\Gamma(\sigma)$, analogous to thermodynamic density of states, is an important quantity, which determines the relation between the mean reduced entropy $\sigma(\tau)$ and the reduced entropic temperature, τ.

5.5. *Improvements*

The computational efficiency of the method depends on two factors. (*a*) Calculating the entropy change in a single sign flip or phase jump is very much less costly than the four or more fast Fourier transform steps needed in one iteration of a static entropy optimization. (*b*) The number of unproductive events is wastefully high, as in other stochastic methods. Improved temperature control and mode selection still allow great scope for improvement, and large three-dimensional problems may be feasible. As yet, the computer program is primitive, and many easy technical improvements can be made.

Two of the more fundamental approximations need to be reviewed. The first was to set the amplitudes of inactive modes to zero, rather than use a well optimized maximum-entropy map at each step. The second was to use a modified entropy function at each grid point that had a negative probability density. This is intuitively reasonable but lacks statistical justification. An alternative would be to use exponential modelling (Collins, 1982) at each step, which avoids negative densities, but add in an *R*-factor penalty. Yet another approach would be to allow a weak source of fictitious negative scatterers.

Entropy dynamics is no better than other annealing methods at recovering from wrong decisions at the top of the cooling sequence. Multiple starting points and an intelligent tree search need to be added.

5.6. *Special significance of entropic temperature*

One unique feature of entropy dynamics is the analogy between the dynamical Boltzmann factor $\exp(NS/\theta)$ for a phase set at an entropic temperature θ, and the joint probability $\exp(NS)$ for the same phases in the statistical theory of random point atoms. Varying the entropic temperature is analogous to altering N, the effective number of atoms.

5.7. *Comparison with R-factor dynamics*

An important feature which distinguishes entropy dynamics from other stochastic methods is the treatment of the Fourier amplitudes. In the present model the active amplitudes are constrained exactly to their known experimental values and the phases are completely free, but there is no constraint of atomicity. This means that the crystallographic *R* factor of the model system (Blundell & Johnson, 1976) is zero, but the densities may be non-physical and negative. The phase system can therefore pass freely through a non-physical state to tunnel from one feasible solution to another. Most other dynamical or Monte Carlo methods sample feasible atomic or molecular model densities with partially incorrect amplitudes, and seek to lower the *R* factor. Examples are molecular dynamics (Brünger, Kuriyan & Karplus, 1987; Kuriyan, Brünger, Karplus & Hendrickson, 1989), hard-sphere solvent-region dynamics (Subbiah, 1991), and fictitious gas atoms with *R*-factor potentials (Semenovskaya, Khachaturyan & Khachaturyan, 1985).

5.8. *How correct is the maximum-entropy solution?*

The example of bacteriorhodopsin gives a simple illustration that the maximum-entropy sign combinations, for a restricted set of strong reflections, with no further amplitude information given, can be seriously wrong. On the other hand, when all the weaker reflections were clamped with their correct signs to provide extra information, the maximum-entropy signs for the strong modes matched the correct solution perfectly. Other trials showed that the correct solution is usually near the top of the empirical entropy distribution. Are these results general? The most important question, still unanswered, is whether the maximum-entropy solutions and the correct solution are the same in essentials, when the full set of known amplitudes is considered.

Experience with other phasing methods suggests that the maximum-entropy solutions, if obtainable, must converge to correct phases when the constraints are over-determined: that is, when the number of known amplitudes greatly exceeds the number of atomic degrees of freedom, $3N$ (Sheldrick, 1990).

References

ABRAGAM, A. (1961). *Principles of Nuclear Magnetism*. Oxford Univ. Press.

ALLEN, M. P. & TILDESLEY, D. J. (1987). *Computer Simulation of Liquids*. Oxford Univ. Press.

BLUNDELL, T. L. & JOHNSON, L. N. (1976). *Protein Crystallography*. London: Academic Press.

BRICOGNE, G. (1984). *Acta Cryst.* A**40**, 410–445.

BRICOGNE, G. (1988). *Acta Cryst.* A**44**, 517–545.

BRICOGNE, G. & GILMORE, C. J. (1990). *Acta Cryst.* A**46**, 284–297.

BRÜNGER, A. T., KURIYAN, J. & KARPLUS, M. (1987). *Science*, **235**, 458–460.

BULLOUGH, P. A. & HENDERSON, R. (1990). *Biophys. J.* **58**, 705–711.

COLLINS, D. M. (1982). *Nature (London)*, **298**, 49–51.

DONG, W., BAIRD, T., FRYER, J. R., GILMORE, C. J., MACNICOL, D. D., BRICOGNE, G., SMITH, D. J., O'KEEFE, M. A. & HOVMOLLER, S. (1992). *Nature (London)*, **355**, 605–609.

GIACOVAZZO, C. (1980). *Direct Methods in Crystallography*. London: Academic Press.

GILMORE, C. J., BRICOGNE, G. & BANNISTER, C. (1990). *Acta Cryst.* A**46**, 297–308.

GILMORE, C. J., HENDERSON, A. N. & BRICOGNE, G. (1991). *Acta Cryst.* A**47**, 842–846.

GULL, S. F. & DANIELL, G. J. (1978). *Nature (London)*, **272**, 686–690.

GULL, S. F., LIVESEY, A. K. & SIVIA, D. S. (1987). *Acta Cryst.* A**43**, 112–117.
HAMMING, R. W. (1986). *Coding and Information Theory*, p. 97. Englewood Cliffs, NJ: Prentice-Hall.
HENDERSON, R. (1977). *Annu. Rev. Biophys. Bioeng.* **6**, 87–109.
HENDERSON, R. & UNWIN, P. N. T. (1975). *Nature (London)*, **257**, 28–32.
HILL, T. L. (1956). *Statistical Mechanics*. New York: McGraw-Hill.
JAYNES, E. T. (1957*a*). *Phys. Rev.* **106**, 620–630.
JAYNES, E. T. (1957*b*). *Phys. Rev.* **108**, 171–190.
JAYNES, E. T. (1983). *Papers on Probability, Statistics and Statistical Physics*, edited by R. D. ROSENKRANTZ. Dordrecht: Reidel.
KARLE, J. & HAUPTMAN, H. (1950). *Acta Cryst.* **3**, 181–187.
KIRKPATRICK, S., GELATT, C. D. & VECCHI, M. P. (1983). *Science*, **220**, 671–680.
KLUG, A. (1958). *Acta Cryst.* **11**, 515–543.
KURIYAN, J., BRÜNGER, A. T., KARPLUS, M. & HENDRICKSON, W. A. (1989). *Acta Cryst.* A**45**, 396–409.
LEVINE, R. D. (1980). *J. Phys. A*, **13**, 91–108.
LEVINE, R. D. & TRIBUS, M. (1979). Editors. *The Maximum Entropy Formalism*. Cambridge, MA: MIT Press.
LEVINTHAL, C. (1968). *J. Chim. Phys.* **65**, 44–45.
LEVITT, M. (1982). *Annu. Rev. Biophys. Bioeng.* **11**, 251–271.
MCCAMMON, J. A. & HARVEY, S. C. (1987). *Dynamics of Proteins and Nucleic Acids*. Cambridge Univ. Press.
MCLACHLAN, A. D. (1989). *Maximum Entropy and Bayesian Methods*, edited by J. SKILLING, pp. 241–249. Dordrecht: Kluwer.
MAIN, P. (1977). *Acta Cryst.* A**33**, 750–757.
METROPOLIS, N., ROSENBLUTH, A. W., ROSENBLUTH, M. N., TELLER, A. H. & TELLER, E. (1953). *J. Chem. Phys.* **21**, 1087–1092.
NAVAZA, J. (1985). *Acta Cryst.* A**41**, 232–244.
PRESS, S. J. (1989). *Bayesian Statistics: Principles, Models and Applications*. New York: John Wiley.
PRINCE, E., SJÖLIN, L. & ALENLJUNG, R. (1988). *Acta Cryst.* A**44**, 216–222.
SEMENOVSKAYA, S. V., KHACHATURYAN, K. A. & KACHATURYAN, A. G. (1985). *Acta Cryst.* A**41**, 268–273.
SHELDRICK, G. M. (1990). *Acta Cryst.* A**46**, 467–473.
SJÖLIN, L., PRINCE, E., SVENSSON, L. A. & GILLILAND, G. L. (1991). *Acta Cryst.* A**47**, 216–223.
SKILLING, J. (1989). *Maximum Entropy and Bayesian Methods*, edited by J. SKILLING, pp. 45–52. Dordrecht: Kluwer.
SKILLING, J. & BRYAN, R. K. (1984). *Mon. Not. R. Astron. Soc.* **211**, 111–124.
SUBBIAH, S. (1991). *Science*, **252**, 128–133.
TOLMAN, R. C. (1938). *The Principles of Statistical Mechanics*. Oxford Univ. Press.
WHITE, P. & WOOLFSON, M. M. (1975). *Acta Cryst.* A**31**, 53–56.
WILKINS, S. W., VARGHESE, J. N. & LEHMANN, M. S. (1983). *Acta Cryst.* A**39**, 47–60.